Available online at www.sciencedirect.com
SCIENCE DIRECT®
International Journal of Solids and Structures 42 (2005) 1381–1399
INTERNATIONAL JOURNAL OF SOLIDS and STRUCTURES
www.elsevier.com/locate/ijsolstr

Compressive response of open cell foams Part II: Initiation and evolution of crushing

L. Gong, S. Kyriakides *

Research Center for Mechanics of Solids, Structures and Materials, The University of Texas at Austin, WRW 110, Austin, TX 78712, USA

Received 29 June 2004; received in revised form 16 July 2004
Available online 18 September 2004

Abstract

Part II of this study is concerned with the understanding and modeling of the nonlinear aspects of the compressive response and crushing of open cell foam. The modeling is based on the anisotropic Kelvin foam developed in Part I assigned the same general geometric characteristics. It is demonstrated that the first knee observed in measured responses is associated with the onset of ligament buckling. Models involving either single or stacks of fully periodic characteristic cells are used to establish the critical stresses in the rise and transverse foam directions. In the rise direction the critical state involves a long wavelength mode whereas in the transverse direction the mode is local to the cell. Postbuckling calculations involving these modes showed the rise direction response to exhibit a limit load which is shown to be imperfection sensitive. The response in the transverse direction is monotonically increasing as observed in the experiments. The crushing response is evaluated by considering finite size microsections which allow localized deformation to develop. Localized crushing is arrested by contact between the ligaments of the buckled cells. Contact is approximated by limiting the amount a cell can collapse in the direction of the applied load. This arrests local collapse and causes it to spread to neighboring material at a nearly constant stress level as in the experiments. The stress picks up when the whole domain has crushed.

Keywords: Open cell foams; Crushing; Mechanical response

1. Introduction

The second part of this two part series of papers is concerned with the understanding and modeling of the compressive response of foam past the initial linearly elastic regime. Fig. 1a shows the compressive

* Corresponding author. Tel.: +1 5124714167; fax: +1 5124715500.
E-mail address: skk@mail.utexas.edu (S. Kyriakides).

0020-7683/$ - see front matter © 2004 Elsevier Ltd. All rights reserved.
doi:10.1016/j.ijsolstr.2004.07.024

stress–shortening response of the 3-ppi polyester urethane foam used in this study (see Table 1 [I]). The specimen was approximately 6 in tall by 12 in square. It was crushed at a constant displacement rate $\dot{\delta}_1/H_1 = 3.8 \times 10^{-3}\ s^{-1}$ along the rise direction. Fig. 1b shows a set of photographs of the specimen during crushing. A separate video camera was used to observe the deformation of the cells on one of the free surfaces of the block. The response has the general characteristics common to all responses reported in Part I. Initially, during the stable branch of the response, the material deforms nearly uniformly. Following the local stress maximum the specimen buckles in an overall manner which can be seen in the configurations as a bowing of the edges on the left and right. This involves local distortion of the cells. As compression progresses, deformation localizes in a banded manner. The bands showed up at what is best described as randomly located sites on the cross section monitored while prevalent characteristic orientation could not be identified. The number of bands grew with time while the stress remained essentially unchanged. At other sites bands broadened and coalesced with neighboring ones. This surface deformation pattern is qualitatively similar to that reported in Wang et al. (2000) who used a digital image correlation technique to establish the evolution of events (see also Bastawros et al., 2000). Although surface deformation patterns do not necessarily represent bulk material behavior, the randomness of the locations of bands is a distinctly different feature from the one or two well-defined collapse fronts seen in in-plane crushing experiments on honeycombs (e.g., Papka and Kyriakides, 1998[I]). This may be a characteristic of the more complex space filling foam microstructure but, more probably, is due to the more random distribution of larger geometric irregularities in foams than in the polymeric honeycomb of Papka and Kyriakides. Despite this difference, during the main evolution of localized deformation, the stress traced essentially a plateau in both cases. At an average "strain" of about 45%, the response develops a positive slope once more.

This general behavior was observed in all five of the foams tested when compressed along the rise direction. As pointed out in Part I, the foam responses were different when compression was applied along their transverse direction. Fig. 7b[I] shows the initial response of the 45 ppi foam to be significantly more compliant (see also Fig. 8a[I]). This trend was captured quite well by the elastic modulus calculations using the anisotropic Kelvin cell. In addition, neither a stress peak nor a stress plateau are traced as the response remains monotonically increasing. Interestingly, the bowing of the sides seen in Fig. 1b did not take place. The block deformed symmetrically with a slight barreling at the top and bottom edges due to friction developed between the foam and the platens. These differences indicate that deformation is probably uniform when the foam is crushed in the lateral direction.

2. Analysis

With this as background we develop a sequence of models and use them to explore the degree to which the large deformation crushing behavior of the foams under uniaxial loading observed in experiments can be reproduced analytically. The microstructure of the model foams will be idealized to be periodic using the space filling Kelvin cell with the geometric characteristics developed in Part I. In other words, the ligaments are assumed to be straight with Plateau border cross sections with the nonuniform cross sectional area distribution given in Eq. (1)[I]. The ligaments will be modeled as shear-deformable beams using ABAQUS's B32 quadratic element. The cell will exhibit the type of anisotropy shown in Fig. 12[I] and Eq. (3)[I] and the relative density quoted will incorporate the correction introduced in Part I for the extra material at the nodes. The basic building block of the models is the characteristic cell shown in Fig. 16[I] with the periodicity conditions given in Eq. (7)[I]. Unless otherwise stated each ligament will have eight elements distributed according to

[I] (•) refers to figures, tables and references in Part I.

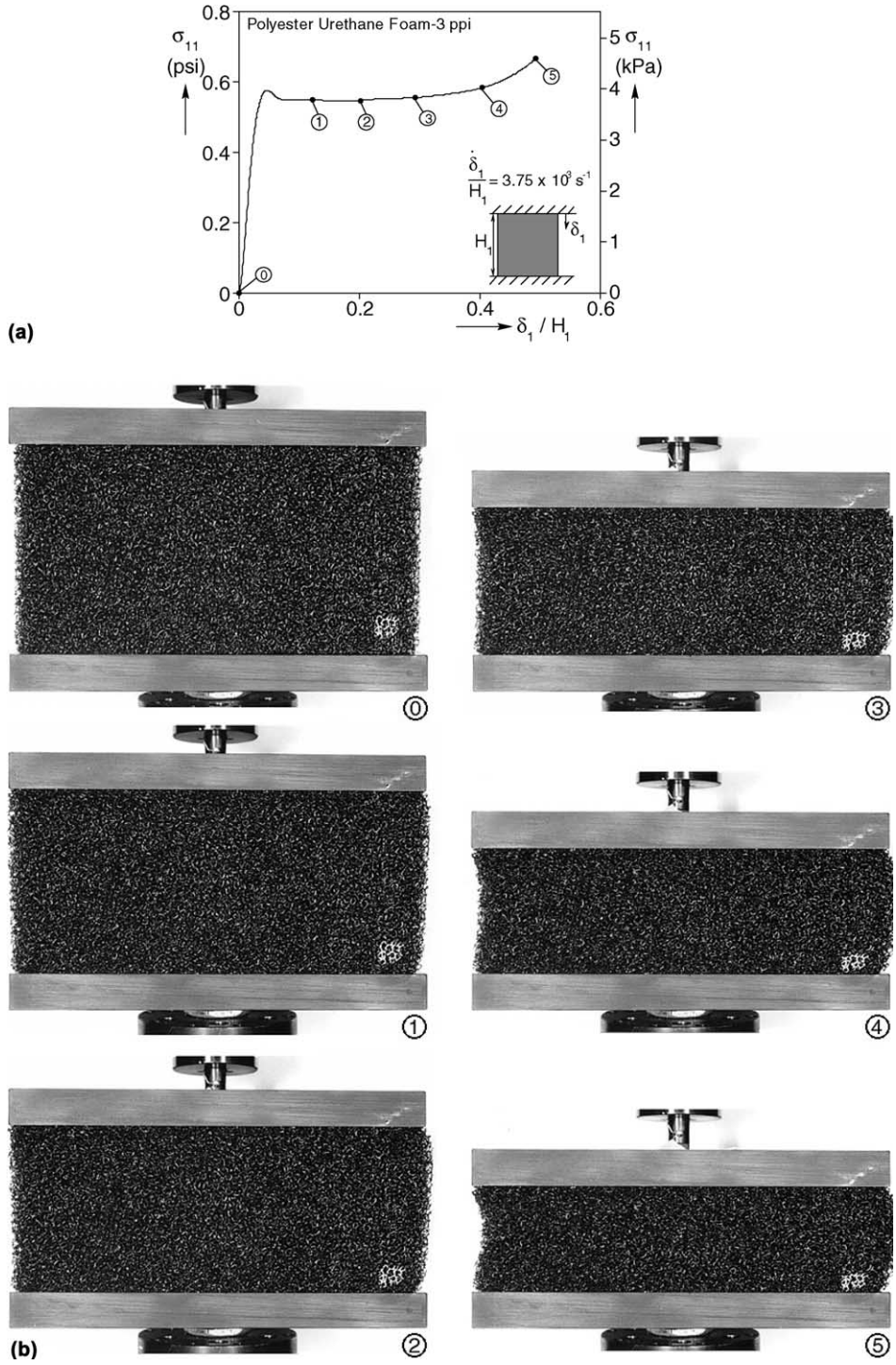

Fig. 1. (a) Compressive stress–shortening response of a polyester urethane foam; (b) sequence of deformed configurations of the foam specimen.

Eq. (8)[I]. The base material is assumed to be linearly elastic, time independent and isotropic with modulus E and Poisson's ratio v (values given in Table 1[I]).

2.1. Initial response and onset of instability

2.1.1. Rise direction

Uniaxial compression of one characteristic cell is accomplished by prescribing incrementally the relative displacement ($\Delta\delta_1$) between the upper and lower periodic boundaries. The average stress σ_{11} required to produce this deformation is the force divided by the initial cross sectional area of the cell ($h_2 \times h_2$—see Fig. 16[I]). Fig. 2a shows the calculated stress–displacement response for an anisotropic foam ($\lambda = 1.3$) with relative density of 0.025. Initially (OAB), the foam deforms uniformly and symmetrically about a vertical

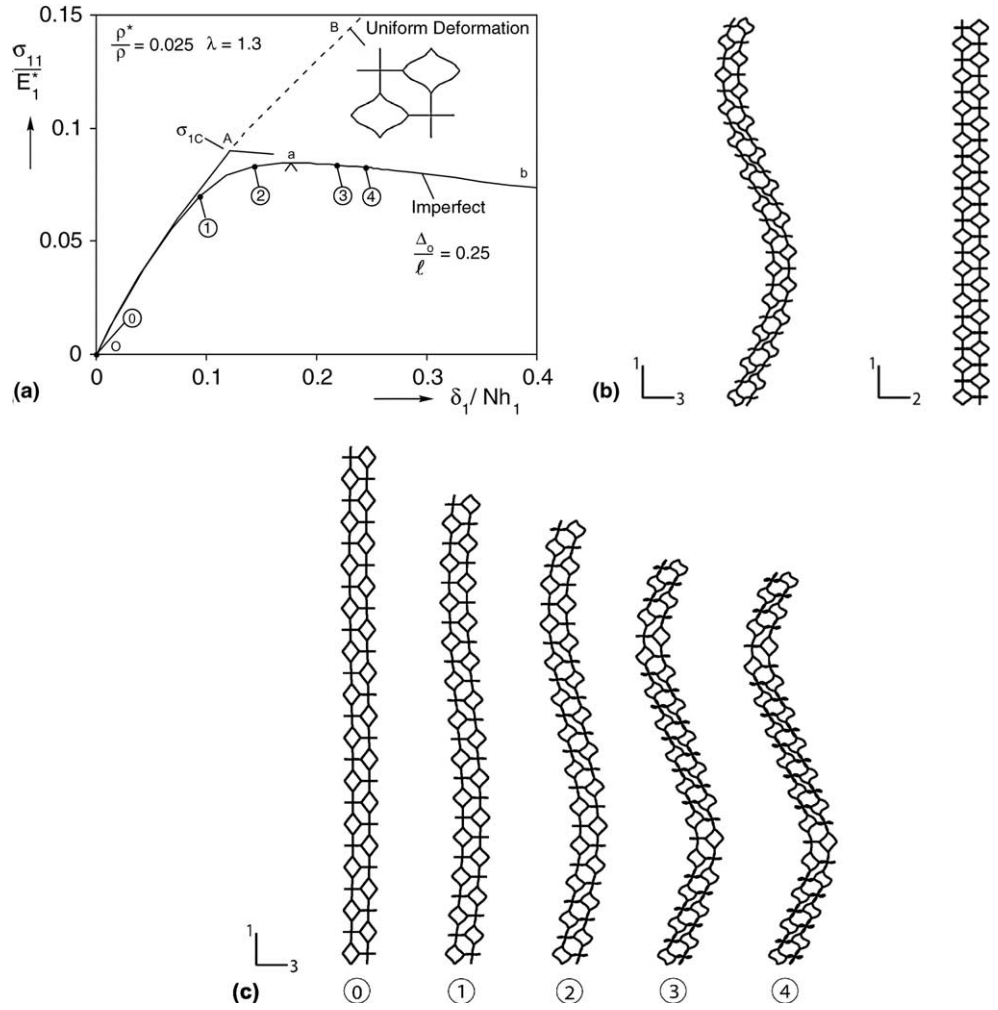

Fig. 2. (a) Calculated rise direction prebuckling and postbuckling stress–shortening responses for fully periodic stacks of Kelvin cells; (b) long wavelength buckling mode of critical stress; (c) sequence of deformed configurations of long wavelength buckling corresponding to points marked on response in Fig. 2a.

axis through the center of the cell (inset shows side view of deformed characteristic cell). The response is stiff but increasingly nonlinear because of the increasingly larger deflections of the ligaments. The foam elastic modulus discussed in Part I corresponds to the slope at the origin and is $E_1^*/E = 0.00176$.

At some point along OAB, an eigen value is identified indicating that an alternate equilibrium configuration is possible. Naturally, because of the size of the domain chosen and the periodicity conditions imposed, this mode of buckling is at the cell level and takes the form shown in Fig. 3 under $N = 1$ and 2. In microstructures with the extent of periodicity such as that of the Kelvin foam, buckling modes involving more than one cell are possible and must be investigated. To this end we conduct similar calculations and eigen value checks for columns of N characteristic cells with periodicity conditions at the top, bottom, and sides. For the present microstructure $N = 2$ yields the same first eigen value and mode but for $N = 3$ the eigen value is smaller and the mode changes to the one shown in Fig. 3. Increasing the number of cells to 4, 6, 8 and 12 reduces further the critical stress and increases the mode wavelength. Fig. 4a illustrates the drop in critical stress with N. For $N > 12$ the critical stress remains unchanged although the mode wavelength increases. Similar calculations are performed for wider columns (number of characteristic cells in directions 2 or 3 is increased). It was found that this does not affect the critical stress or the corresponding mode. The same insensitivity is observed when the column is made wider in both directions. Thus, the critical stress is taken to be the plateau value in Fig. 4a and is identified on the response in Fig. 2a as σ_{1C}.

The behavior described indicates that the periodic foam admits a long wavelength buckling mode rather than one limited to the cell level. This finding is in concert with the bowing observed in the compressed foam block shown in Fig. 1b. The long wave mode is to be contrasted with that of honeycombs under in-plane crushing (Papka and Kyriakides, 1994,1998a) where the buckling mode was at the cell level.

Interestingly the neighborhood just beyond the critical stress contains many eigen values and modes similar to the ones shown in Fig. 3. This richness in closely packed buckling modes is a characteristic which indicates sensitivity to a variety of imperfections, a subject which will be discussed later.

Triantafyllidis and co-workers (Geymonat et al., 1993; Schraad and Triantafyllidis, 1997a,b) have developed an efficient, robust numerical method for establishing the onset of instability in periodic structures under general loading conditions based on Bloch waves. The characteristic cell with the appropriate periodicity conditions is loaded incrementally along a given load path. Using Bloch waves and the stiffness

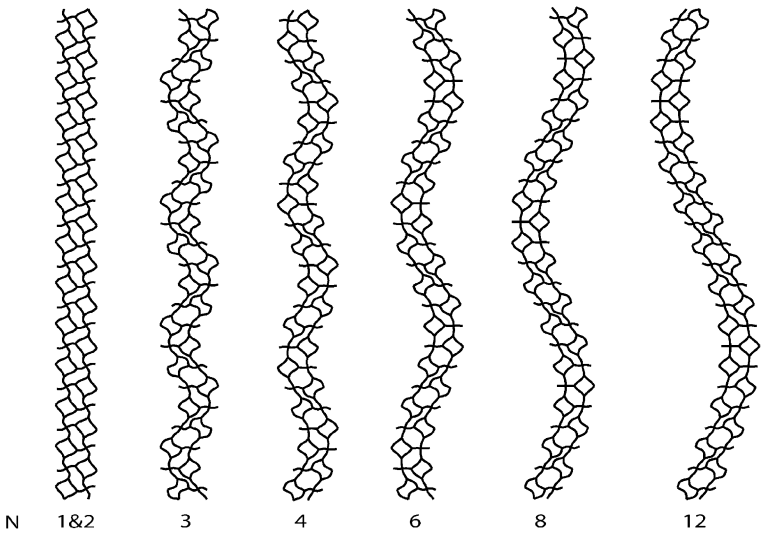

Fig. 3. Buckling modes corresponding to fully periodic stacks of N Kelvin cells.

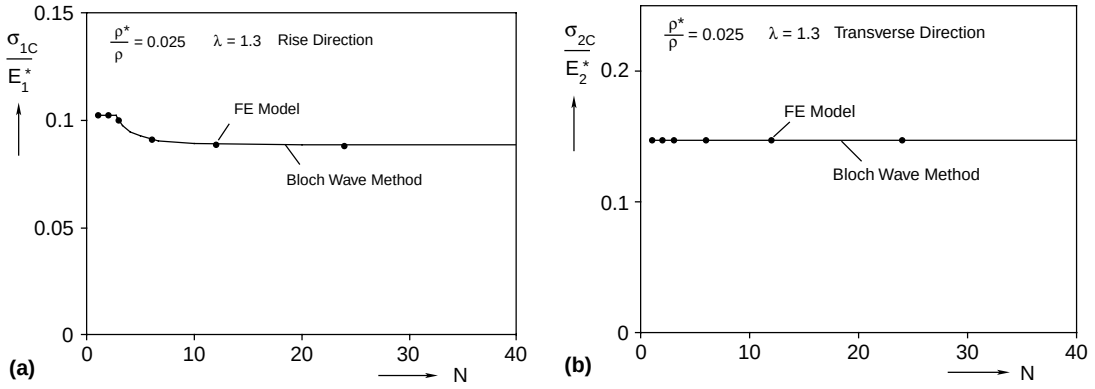

Fig. 4. (a) Critical stress in foam rise direction as a function of number of cells in model analyzed; (b) critical stress in foam transverse direction as a function of number of cells in model analyzed.

matrix of the deformed unit cell, one can investigate the stability of the infinite periodic medium against all possible bounded perturbations and establish the critical condition. The periodicity of our Kelvin cell foam and the numerous checks which must be performed to establish the critical condition make the problem an excellent candidate for application of this method. Details of this application can be found in Gong et al. (submitted for publication). Here we will quote results corresponding to the specific uniaxial loadings considered. For example, results obtained by this method for the specific case discussed above are included in Fig. 4. They are seen to agree perfectly with the discreet results generated by the more laborious method, which is reassuring.

The critical stress was calculated in a similar manner using the characteristic cell model discretized with solid elements described in Section 4.2 of Part I (C3D15V prisms and C3D27 bricks). It was found to correspond to the same long wavelength buckling mode but to be 29.8% lower than the value in Fig. 2. Two main factors contribute to this difference. The first is the more accurate representation of the node compliance afforded by the solid model. The second is related to cell ligament cross sectional distortion resulting from prebuckling bending. The solid model captures this cross sectional distortion whereas beam models do not. As pointed out in Part I, the solid element model is prohibitively computationally expensive. It was thus decided to limit its use to only bifurcation stress calculations for the major cases analyzed.

We next examine the postbuckling response corresponding to the long wavelength mode associated with σ_{1C}. The mode is assigned an amplitude and applied as an initial imperfection to a column of characteristic cells of sufficient height ($N = 12$ is selected here). The periodicity conditions applied to the perfect geometry are maintained. The microsection is then compressed in the x_1-direction by prescribing incrementally δ_1. Results for the case with imperfection amplitude of $\Delta_0/\ell = 0.25$ are included in Fig. 2a ($\Delta_0 = |\boldsymbol{u}_0(\boldsymbol{x})|_\infty$ and $\boldsymbol{u}_0(\boldsymbol{x})$ is the imperfection). The initial and several deformed configurations corresponding to points marked with solid bullets on the response are shown in Fig. 2c. Initially the response follows that of the perfect case. As σ_{1C} is approached, the domain is distorted (see configurations ① and ②) resulting in reduction of its stiffness. With further distortion the imperfect case response increasingly deviates from that of the perfect case and reaches a limit load (stress) at an average strain of about 17.6%. Subsequently, the stress decreases with deformation. The deformed configurations in Fig. 2c show the progressive growth of the buckled configuration. These calculations were performed with just one column of characteristic cells. It is worth noting that increasing the width of the characteristic domain does not change the calculated response.

The fact that a limit load instability is traced in the response of this strictly periodic microstructure, indicates that localized deformation patterns will probably be energetically preferred if the periodicity condi-

tions are relaxed to some degree. This possibility will be examined in the next section. (Note that the possibility of contact between ligaments of deforming cells was precluded in both of these calculations.)

2.2. Transverse direction

We repeat the process for uniaxial compression in the transverse direction (x_2). Again we start with one characteristic cell with periodicity conditions on all of its sides and prescribe incrementally the relative displacement ($\Delta\delta_2$) between the two sides normal to the x_2-direction. The calculated $\sigma_{22}-\delta_2$ response is shown in Fig. 5a. Initially the deformation involves symmetric crushing of the cell as shown in the inset. As mentioned earlier the initial modulus is much smaller than the corresponding one in the rise direction ($E_2^* = 0.475E_1^*$). At larger strains the response again becomes increasingly nonlinear due to geometric distortion of the cells. The first eigen value occurs at point A at a stress of σ_{2C}. Two views of the corresponding

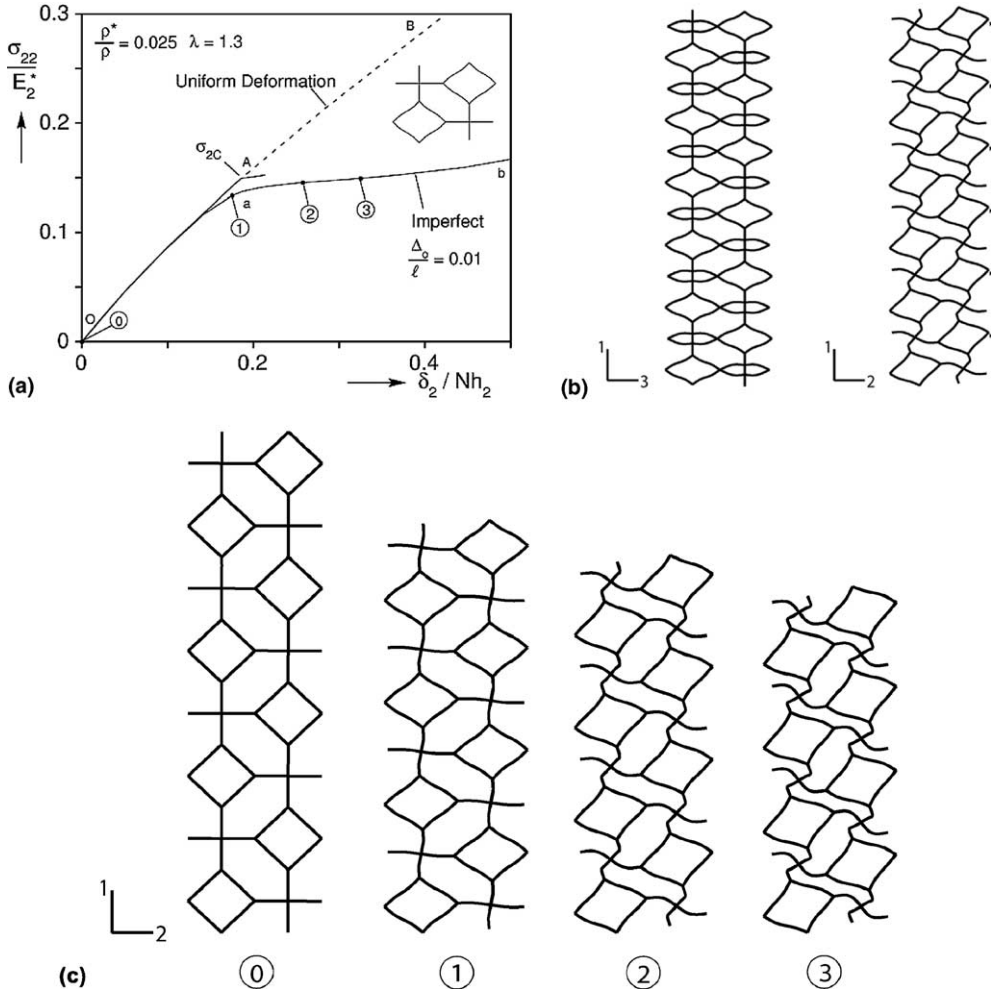

Fig. 5. (a) Calculated transverse direction prebuckling and postbuckling stress–shortening responses for fully periodic Kelvin cells; (b) buckling mode of critical stress limited to cell level; (c) sequence of deformed configurations of cell level buckling corresponding to points marked on response in Fig. 5a.

buckling mode are shown in Fig. 5b. The mode is limited to just one characteristic cell (for clarity the microsection shown includes six cells). The critical stress calculated by the solid FE model was found to be associated with the same local cell mode but to be 27.7% lower than the value in Fig. 5a for the same basic reasons as given for the rise direction.

We next conduct similar compression tests on columns with N characteristic cells where N is progressively increased as described above. Unlike the rise direction, the calculated critical stress and the corresponding mode were found to be insensitive to N. This was also confirmed by using the Bloch wave method. Results of σ_{2C} predicted by the two methods are compared in Fig. 4b and seen to be in excellent agreement. The critical stress and mode were also found to be insensitive to the width of the column analyzed. This implies that in this direction the prevalent buckling mode is the local one shown in Fig. 5b.

The buckling mode corresponding to σ_{2C} with amplitude $\Delta_0 = 0.01\ell$ is now applied as an imperfection to the characteristic cell and the compression test is repeated keeping the same periodicity conditions. The imperfect cell response initially follows that of the perfect one. It starts to deviate from it as σ_{2C} is approached. Deformed configurations corresponding to points marked on the response are shown in Fig. 5c. In configuration ① nonsymmetric deformation is visible and it is seen to grow in configurations ② and ③. In contrast to the rise direction, this response maintains a positive slope to large values of average strain. We note again that increasing the width of the characteristic domain does not alter the response. This overall behavior indicates that this deformation pattern will also be maintained in a larger domain in which the periodicity conditions are relaxed.

In summary, the compressive behaviors in the rise and transverse directions of the anisotropic Kelvin foam are distinctly different. In the rise direction the foam buckles into a long wavelength mode. The postbuckling behavior of this mode exhibits a limit load instability which in a less constrained domain is expected to result in localized collapse. Both the long wave buckling mode and localized crushing were observed in the rise direction crushing tests on the five foams tested. In the transverse direction the critical buckling mode is at the cell level and the postbuckling response is monotonically increasing and stable. These general features were also observed in the transverse direction crushing experiments. The long wavelength buckling mode was absent and the response remained a monotone.

2.3. Isotropic foam

In view of the differences introduced by anisotropy to the idealized foam, it is worthwhile to also examine the compressive behavior of the isotropic case ($\lambda = 1$). The compressive response of the perfect case is shown in Fig. 6a. The initial elastic modulus is $E^*/E = 0.001123$ which lies between the E_1^* and E_2^* values calculated for $\lambda = 1.3$. The critical stress is found to correspond to a long wavelength mode. Fig. 7 shows how σ_C varies with the number of cells in the column analyzed. The buckling stress drops as N increases but at a much slower rate than it did for the anisotropic case. For $N > 12$ the buckling stress does not change. The buckling mode corresponding to $N = 12$ shown in Fig. 6b is similar to the one seen earlier in Fig. 2b. As in the other two cases, the critical stress yielded by the solid FE model is 17.4% lower. The same long wavelength mode shown in Fig. 6b is associated with the critical stress.

Included in Fig. 6a is the compressive response of the imperfect case where the buckling mode for $N = 12$ is used as initial imperfection (amplitude $\Delta_0 = 0.45\ell$). The response exhibits a limit load indicating again that localized crushing can be expected to take place in the isotropic foam also.

The onset of instability in Kelvin cell foams was previously investigated by Laroussi et al. (2002). Their foam was linearly elastic, isotropic, with ligaments of uniform circular cross section. The ligaments were modeled as shear-deformable beams. In most calculations the foam had a relative density of 0.06. The characteristic cell adopted was somewhat different from the one used in this study but, because in most stability calculations an assemblage of such cells was used, this difference may be inconsequential. The main thrust of the work was the use of a variation of the Bloch wave theory of Triantafyllidis et al. to establish stability

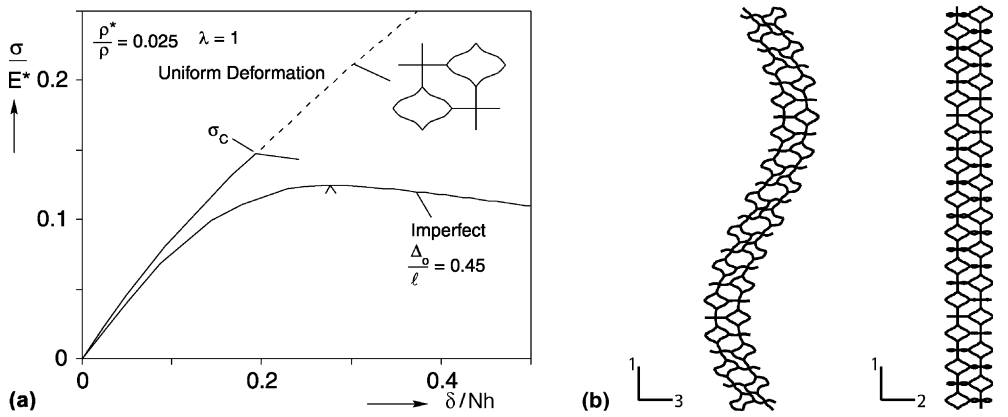

Fig. 6. (a) Calculated prebuckling and postbuckling stress–shortening responses for fully periodic stacks of isotropic Kelvin cells; (b) Long wavelength buckling mode of critical stress.

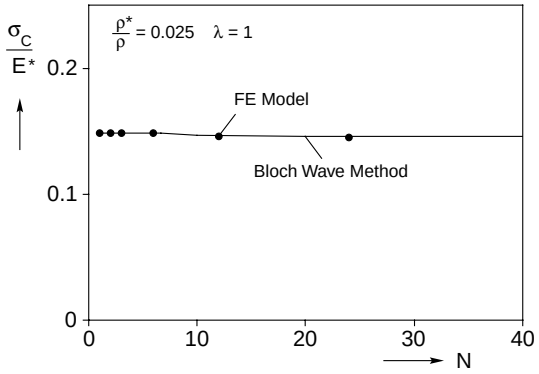

Fig. 7. Critical stress of isotropic foam as a function of number of cells in model analyzed.

envelopes in different multiaxial spaces. Uniaxial compression was also discussed and a long wavelength buckling mode was found to occur. The postbuckling behavior of this case was not discussed. Because of the many differences in the assumed microstructure and in the modeling scheme adopted, direct comparison with the present results is difficult and will not be attempted. In the cases discussed by these authors, perturbation was applied to the initial geometry rather than the deformed one. Since instability occurs at average strains well beyond 10% this will contribute to some difference between the critical stresses yielded by their scheme and the present one.

2.4. Parametric study of critical stress

The procedure described in the previous section was used to calculate the critical bifurcation stress as a function of the geometric parameter r_0/ℓ for foams of anisotropy values λ ranging from 1 to 1.4. The variable r_0/ℓ was varied so that the relative density ρ^*/ρ was in the range of 0.01–0.06. In all cases the ligament cross sectional variation was in accordance with $f(\xi)$ in Eq. (1)[I]. As a result, ρ^*/ρ is related to r_0/ℓ through a powerlaw with the constants given in Table 3[I]. The calculated critical stresses were fitted to powerlaw expressions as follows:

$$\frac{\sigma_C}{E} = k_{\bar{r}}\left(\frac{r_0}{\ell}\right)^{n_{\bar{r}}} \quad \text{and} \quad \frac{\sigma_C}{E} = k_{\bar{\rho}}\left(\frac{\rho^*}{\rho}\right)^{n_{\bar{\rho}}} \tag{1}$$

Critical stresses calculated for two representative cases ($\lambda = 1$ and 1.3) for the rise direction (σ_{1C}) are plotted in log–log scales against r_0/ℓ in Fig. 8. The plots confirm that the critical stress is indeed a powerlaw function of r_0/ℓ. The numerical results of the fits are listed in Table 1. It is of interest to observe that in the corresponding strictly linear problem $n_{\bar{r}} = 4$. If in addition the material distribution at the nodes is neglected then $n_{\bar{\rho}} = 2$ as suggested by Gibson and Ashby (1982, 1997)[I]. By contrast, in the present calculations $n_{\bar{r}} < 4$ because of the problem nonlinearity. In addition, $n_{\bar{\rho}} > 2$ and both depend on the anisotropy variable λ.

It is of interest to compare the critical bifurcation stresses calculated for the five foams tested with the measured limit stresses (σ_I in Table 1[I]). The calculated and measured values are listed in Table 2. In all cases the predicted critical stress is higher by about a factor of 2 which is not surprising. The actual microstructure is irregular and has significant geometric imperfections. In addition, tests in which the foam is compressed between rigid platens mask to some degree the actual compressive strength because of the interaction between the edges of the foam and the platens. Another factor contributing to this difference are idealizations introduced by the beam models which make the microstructure stiffer. As demonstrated above, solid FE models which are more representative of actual foams yield lower critical stresses.

The limit stress of the imperfect microstructure is a more realistic estimate of the maximum load capacity of the material. It is thus worth establishing its imperfection sensitivity. Fig. 9a shows for example how the imperfection amplitude affects the response of the case analyzed in Fig. 2. Increase of the imperfection makes the microstructure more compliant and lowers the limit load. The limit stress (σ_{1L}) from similar calculations normalized by the bifurcation stress of the perfect structure is plotted against (Δ_0/ℓ) in Fig. 10 (dashed line). Its imperfection sensitivity is seen to be quite significant.

Calculations of imperfect microstructures similar to the ones presented in Fig. 9 were performed for the five foams used in the experiments (using their individual values of r_0/ℓ and λ). In each case the imperfection corresponded to the mode of the critical stress but its amplitude, Δ_0, was varied. The calculated limit stresses are plotted against Δ_0/ℓ in Fig. 10. The imperfection sensitivity of the normalized limit stress of the different foams is seen to be similar.

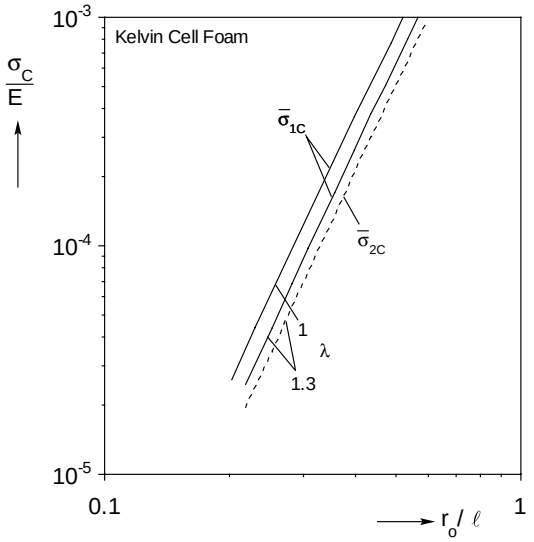

Fig. 8. Calculated critical stress of isotropic and anisotropic foams as a function of geometric parameter r_0/ℓ.

Table 1
Fit parameters for powerlaw relationships between the critical stress (σ_{1C}) and r_0/ℓ and ρ^*/ρ

λ	$n_{\bar{r}}$	$k_{\bar{r}}$	$n_{\bar{\rho}}$	$k_{\bar{\rho}}$
1	3.8071	0.011918	2.272	0.6825
1.1	3.8447	0.011241	2.288	0.7286
1.2	3.8612	0.010184	2.298	0.7425
1.3	3.8712	0.009122	2.299	0.7577
1.4	3.8842	0.008414	2.307	0.7185

Table 2
Comparison of measured and calculated critical stresses for rise direction

Foam ppi	λ	$\frac{\rho^*}{\rho}$ (%)	$\frac{\sigma_{1I}}{E}\times 10^3$	$\frac{\sigma_{1C}}{E}\times 10^3$	$\frac{\sigma_{1L}}{E}\times 10^3$ ($\Delta_0/\ell=1$)	$\frac{\sigma_{1L}}{E}\times 10^3$ ($\Delta_0/\ell=2$)
3	1.432	2.18	0.0556	0.1083	0.0841	0.0681
10	1.360	2.47	0.0619	0.1466	0.1187	0.1000
20	1.281	2.36	0.0679	0.1350	0.1097	0.0923
45	1.256	2.44	0.0800	0.1459	0.1183	0.0993
100	1.233	2.82	0.0867	0.2054	0.1656	0.1384

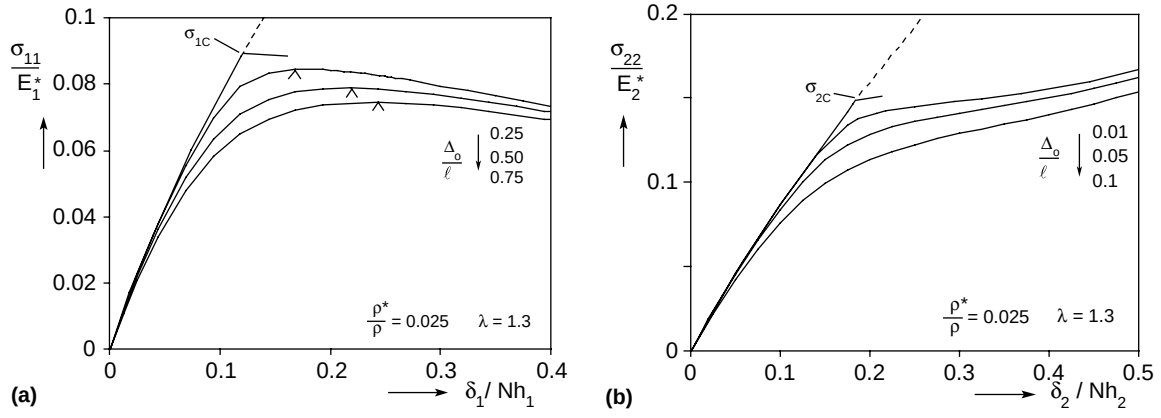

Fig. 9. Stress-shortening responses for fully periodic stacks of Kelvin cells for different imperfection amplitudes: (a) rise direction; (b) transverse direction.

Included in Table 2 are calculated limit stresses for the five foams tested for imperfection amplitudes of $\Delta_0/\ell = 1$ and 2. The predictions are now seen to be much closer to the measured values approaching them from above. This illustrates that an even more accurate prediction of the measured initiation stress will have to involve models with a more accurate representation of the actual microstructure with all its imperfections.

A similar parametric study was conducted for the bifurcation stress in the transverse direction (σ_{2C}). In all cases the mode corresponding to the critical stress was local to the characteristic cell (similar to results in Fig. 5). A sample of σ_{2C} results for $\lambda = 1.3$ are plotted against r_0/ℓ in Fig. 8. They are lower than the corresponding σ_{1C} values but have nearly the same exponent $n_{\bar{r}}$.

Transverse direction buckling stresses were also calculated for each of the five foams used in the experiments. Since no limit stress was traced in the experimental responses from this direction (see Fig. 8a[I]), the

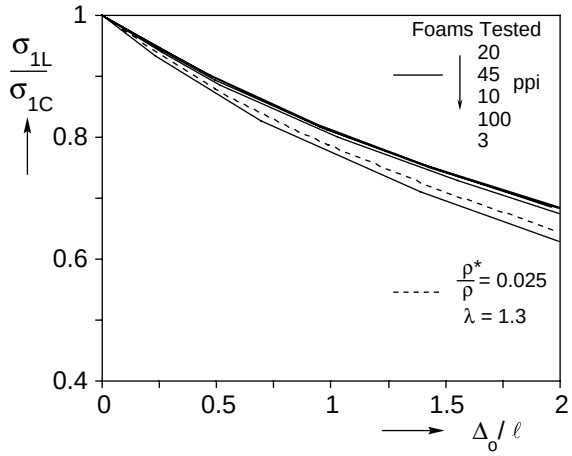

Fig. 10. Calculated limit stress of foams used in the experiments as a function of imperfection amplitude.

buckling stress was estimated by the following construction. The initial linearly elastic part of the response was extrapolated and the relatively linear part of the response just after the first knee was also fitted linearly. The stress at the intersection of the two lines was taken to represent a lower bound estimate of the material buckling stress.

The stresses estimated in this manner are listed under σ_{2I} in Table 3. They are lower than the corresponding σ_{1I} by factors ranging approximately between 2 and 4. The calculated critical stresses listed under σ_{2C} in Table 3 are higher than these experimental values by about a factor of two; in other words, their difference is of the same order of magnitude as seen in the results in the rise direction in Table 2. The main cause of this difference is again attributed to the irregularity of the actual foam microstructure.

Fig. 9b shows how the amplitude of the initial imperfection affects the postbuckling response in the transverse direction. The behavior is typical of structures with a stable postbuckling behavior. The imperfection makes the response more compliant. It rounds and lowers the knee in the neighborhood of the bifurcation point. In view of the results we conclude that the difference between the calculated bifurcation stress and the experimental knee stress can again be attributed to geometric imperfections including the irregularity of the microstructure of the actual foams.

2.5. Crushing response

Calculations which go well beyond the onset of instability discussed above must address two important new aspects of the problem. The first is the complication introduced by the eventual contact between the buckling ligaments of the cells. The second issue affects cases where a limit load instability was recorded

Table 3
Comparison of measured and calculated transverse direction critical stresses

Foam ppi	λ	$\frac{\rho^*}{\rho}$ (%)	$\frac{\sigma_{2I}}{E} \times 10^3$	$\frac{\sigma_{2C}}{E} \times 10^3$
3	1.432	2.18	0.03395	0.1062
10	1.360	2.47	0.05216	0.1093
20	1.281	2.36	–	0.1065
45	1.256	2.44	0.06636	0.1175
100	1.233	2.82	0.05679	0.1687

in the characteristic section analysis. In such cases localized deformation is a strong possibility. Thus, the domain analyzed must be altered/expanded to allow for localization to develop. Both issues bring challenges to the modeling effort and we will address each separately.

2.6. Ligament contact

As was clearly demonstrated in our studies of honeycomb crushing, contact between the collapsing walls of cells play a pivotal role in the load plateau traced under displacement controlled compression. Contact arrests local collapse and, as a consequence, locally stabilizes the microstructure. This in turn causes cells adjacent to the zone of local collapse, hitherto only slightly deformed, to start collapsing. This process repeats until collapse spreads in this manner to the whole specimen. Although less ordered, local collapse of zones of cells also governs the crushing of foams. Experimental observations have also confirmed that collapse of these zones is again terminated by contact between the buckled ligaments. The irregularity of the foam microstructure makes modeling of ligament contact formidable. Indeed, despite the simplifications introduced to the modeling effort by the adoption of the periodic Kelvin cell, modeling of ligament contact remains a difficult task which often results in numerical convergence difficulties. We bypassed this difficulty by adopting the following approximation for ligament contact. The corner nodes of all vertical rhombi (squares for $\lambda = 1$) are connected with springs. Thus, for example, points a and c in rhombus abcd highlighted in Fig. 11 are connected. The springs (ABAQUS SPRING2) become activated when the vertical distance between the two nodes exceeds a chosen threshold. Once activated the spring force depends only on the vertical distance of the connected nodes; in other words, relative displacement of the nodes in the x_2–x_3 plane is uninhibited. Thus the force in the spring is given by

$$F = \begin{cases} 0, & u_{1c} - u_{1a} < \psi, \\ k(u_{1c} - u_{1a}), & u_{1c} - u_{1a} \geqslant \psi, \end{cases} \tag{2}$$

where ψ is the gap that must be closed first before the spring is activated and k is the spring constant. The selection of the variables ψ and k and their effects on the results will be discussed below.

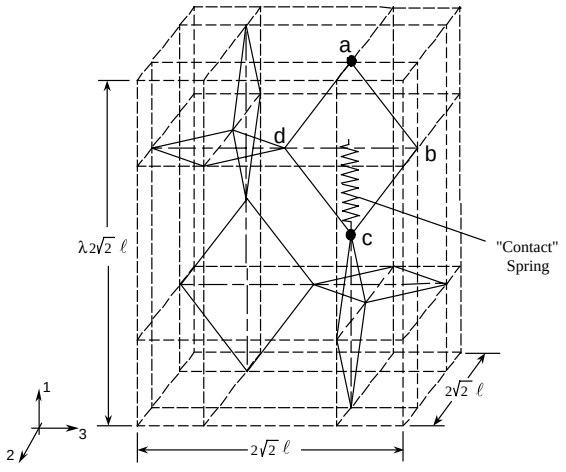

Fig. 11. Characteristic cell showing placement of a "contact" spring introduced in direction of loading in a typical vertical rhombus.

2.7. Crushing of a finite size foam domain

We now explore the possibility of the model foam developing deformation patterns precluded by the full periodicity conditions prescribed in the previous section. To this end we continue to consider foam with relative density of 0.025 and the same anisotropy of $\lambda = 1.3$. Because of limitations imposed by our computer facilities, we choose a domain with eight characteristic cells in the rise direction (12 would have been more optimal) and 28 in the transverse direction (x_3) (see undeformed configuration, ⓪, in Fig. 12b). The domain is one characteristic cell thick (x_2-direction) with periodicity conditions applied to the front and back surfaces. Periodicity conditions are also assumed at the top and bottom edges. Compression is applied along the rise direction by prescribing incrementally the relative displacement between the upper and lower edges. The main difference from calculations in the previous section is that the domain width is finite as the two lateral edges are now let free. An initial imperfection (amplitude $\Delta_0 = 0.197\ell$) corresponding to the critical mode of the fully periodic microstructure (of this height) is introduced to the model. (Note that the critical stresses of the fully periodic foam and of the one with its sides free are very close.) In addition, the pseudo-contact scheme described above with the parameters $\psi = 0.871\ell$ and $k = 0.202C_A E r_0^2/\ell$ was implemented.

Fig. 12a shows the calculated average stress–displacement response and Fig. 12b shows the undeformed and a sequence of deformed configurations corresponding to the points on the response marked with numbered flags. The initial response follows the trivial one closely. At higher stress levels the imperfection is excited (see configuration ①) and nontrivial deformation grows causing a softening in the response. This results in a stress maximum close to configuration ②. As might be expected, freeing the lateral ends makes the limit stress about 5% lower than the corresponding value for the fully periodic domain with the same imperfection value. Subsequent to the stress maximum localized deformation starts to become visible in the concave parts of the free ends in configuration ③. At these sites deformation grows to levels which cause the contact springs to be activated. Further local deformation is then inhibited and collapse spreads across to neighboring cells. By configuration ④ highly deformed zones and less deformed ones are distinctly seen in the domain. As this continues contact springs are activated in increasingly more cells resulting in the upturn in the average stress seen to occur around a normalized displacement of 45%.

Drawn with a dashed line in Fig. 12a is the corresponding response calculated in the absence of the contact springs. A set of deformed configurations corresponding to the points marked on this response is shown in Fig. 12c. The two responses are identical up to the limit stress. Thus, the initial and the first two deformed configurations in Fig. 12b and c are identical. Following the limit stress, localization starts at the same sites in both models in the concave parts of the free ends. In the absence of the artificial contact, localization results in penetration of the deforming cells which starts to be seen in configuration 3 in Fig. 12c. Penetration continues in configurations 4 and 5. Clearly penetration, as it develops in this setting, has no stabilizing effect. As a result, firstly the stress keeps decreasing monotonically and secondly the spreading of deformation to neighboring regions observed in Fig. 12b does not materialize. The free ends have some effect on the two sets of results presented in Fig. 12. This effect can be reduced by increasing the width of the microsection.

The variable ψ in Eq. (2) governs the extent to which individual cells can collapse. Its influence on the overall crushing response is shown in Fig. 13 for an 8×28 cells model. It has no influence in the early stages of deformation and on the limit stress which is governed instead by the imperfection amplitude. Increasing ψ extends the stress plateau and delays the densification stage of the response. In other words, ψ influences the energy absorption capacity of the foam. Other features of the crushing response remain similar to those of the case presented in Fig. 12a and b. In the present modeling scheme the value of ψ is chosen so that the experimental values of $\Delta\varepsilon^p$ are matched.

In the transverse direction the response of the fully periodic model is monotonic. Thus, it does not have the natural tendency to collapse and localize. This was confirmed by analyzing finite size microsections

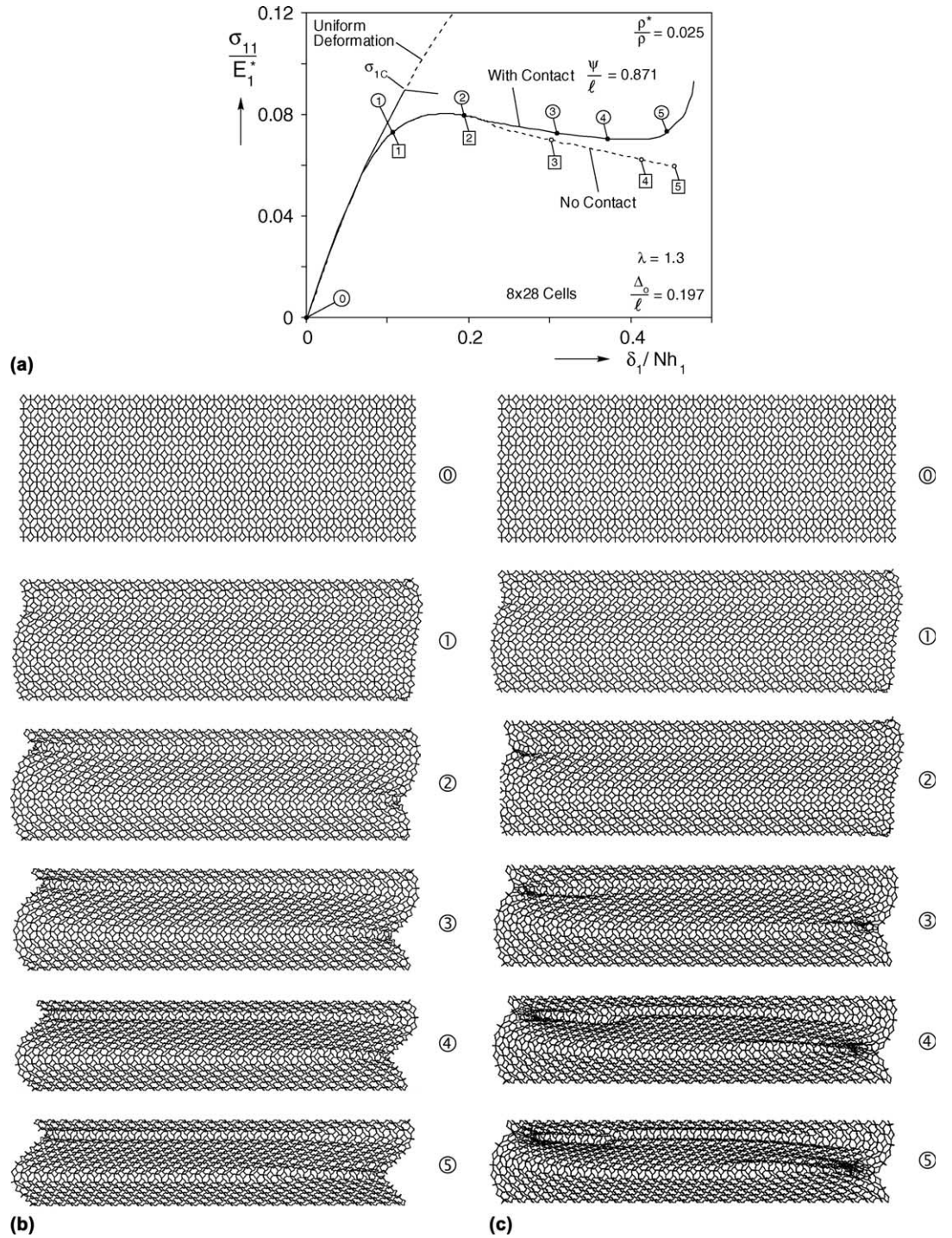

Fig. 12. (a) Stress–displacement responses of a finite size foam microsection with and without contact springs; (b) sequence of deformed configurations corresponding to response in (a) in the presence of contact springs; (c) sequence of deformed configurations corresponding to response in (a) in the absence of contact springs.

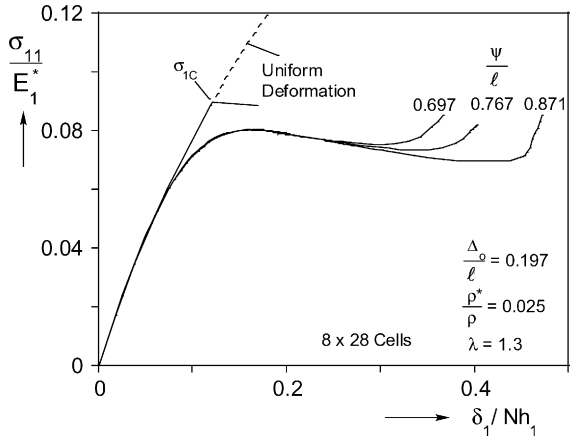

Fig. 13. Crushing responses of a finite size foam microsection for different values of contact variable ψ.

(6×16 cells) similar to the ones described above. The local cell mode of Fig. 5c is repeated in all cells with the exception of a narrow boundary layer along the free ends. Away from the ends ligament contact does not occur until an average strain has gone passed 40%. The fully periodic response is thus representative of finite size specimens also up to this strain level.

In the results shown this far nontrivial deformation was activated by an imperfection corresponding to the mode of the critical stress. It was noted earlier that the Kelvin cell foams analyzed were found to have quite a large number of eigen values at stresses only slightly higher than the critical stress. This richness in closely packed eigen values and modes indicates that the idealized microstructure may be sensitive to a variety of imperfections. To test this we compressed finite size microsections similar (8×12 cells) but with an initially perfect geometry. These microsections were "disturbed" by two equal and opposite point side forces of small amplitude applied at different heights along the two free sides. Fig. 14a shows stress–axial shortening responses for three such models identified as "I", "II" and "III", disturbed at different locations. The location of the applied point forces is shown in the single deformed configurations from each case in Fig. 14b. The disturbances destabilized each model at a stress level close to the critical stress of the perfect case. The three responses are close to each other and exhibit a limit load following which deformation localizes. The localization is illustrated in the individual configurations in Fig. 14b which correspond to points soon after the respective limit stress. When contact springs are included in such models continued compression results in stress plateaus such as the one in Figs. 12a and 13. The results demonstrate that the microstructure is sensitive to a variety of disturbances.

3. Summary and conclusions

Part II of this study is concerned with the understanding and modeling of the nonlinear aspects of the compressive response and crushing of open cell foam. The modeling is based on the anisotropic Kelvin foam developed in Part I assigned geometric characteristics observed in a set of polyester urethane foams analyzed. The ligaments are modeled as shear deformable beams and the base material is assumed to be linearly elastic. Models involving either single or stacks of fully periodic characteristic cells are used to establish the critical stresses in the rise and transverse foam directions. In the rise direction the critical state involves a long wavelength mode whereas in the transverse direction the mode is local to the cell. The critical stresses calculated for the five foams tested follow the same trends as the measured limit stresses

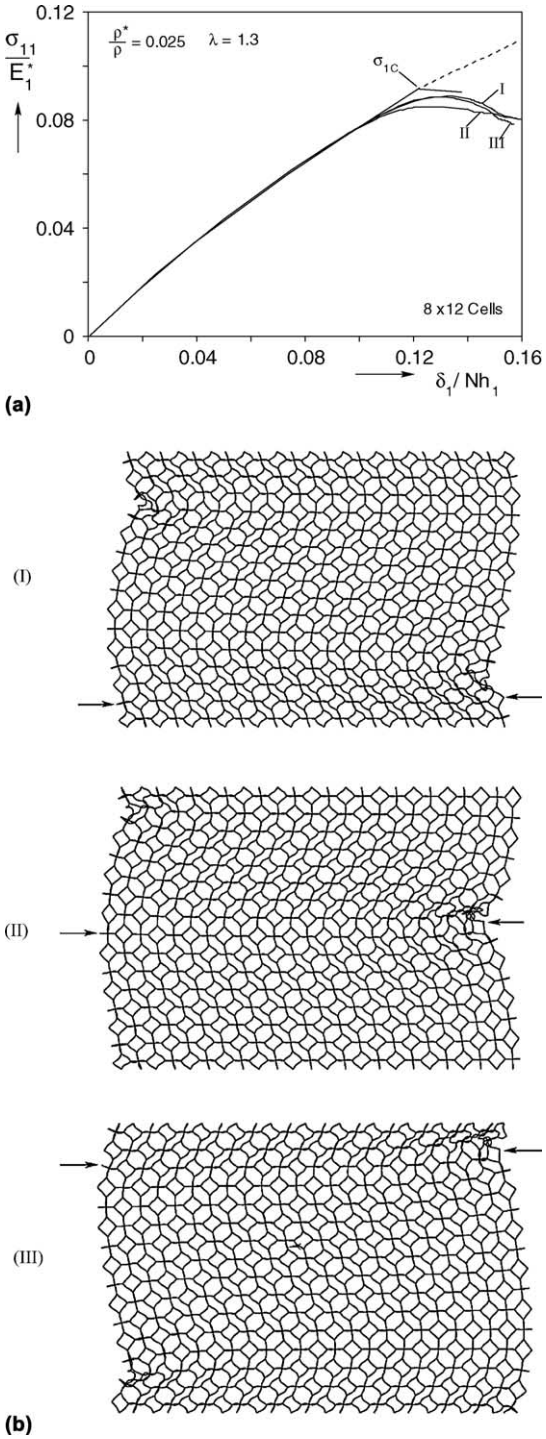

Fig. 14. (a) Stress–displacement responses of finite size foam microsections disturbed by side forces at locations shown in Fig. 14b; (b) deformed configurations corresponding to points just after the limit stresses of responses "I", "II" and "III" in (a).

recorded in the rise direction and the stresses corresponding to the first knee of the transverse direction responses. They are however higher than both sets of measurements by about a factor of 2. Selected calculations in which the foam was discretized with solid FEs instead, yielded 20–30% lower critical stresses. A parametric study of the critical stress revealed it to be a powerlaw function of the geometric parameter r_0/ℓ. The exponent varied with the degree of anisotropy ranging between 3.81 for the isotropic case and 3.88 for $\lambda = 1.4$.

Postbuckling calculations were conducted involving fully periodic microsections with initial imperfections corresponding to the mode of the respective critical stress. In the rise direction such a response exhibits a limit load which is shown to be imperfection sensitive. Calculations involving realistic imperfection amplitudes yield limit stresses which are much closer to the initiation stresses measured in the five foams tested. The presence of a limit stress in the response as well as the long wavelength buckling mode are in agreement with experimental observations.

Similar imperfect cell postbuckling calculations for the transverse direction yield monotonically increasing responses for all values of anisotropy considered ($1 < \lambda \leqslant 1.4$). The monotonicity of the response as well as the absence of long wavelength buckling modes are consistent with transverse direction experimental observations.

The presence of a limit load in the rise direction response of fully periodic microsections indicates that, if some of the periodicity constraints are relaxed, localized deformation may develop. To this end finite size microsections with two lateral sides free were analyzed. Localized collapse develops soon after attainment of the limit load. In the foams tested localized cell crushing is arrested by contact between the ligaments of the buckled cells. In the model contact is approximated by limiting the amount a cell can collapse in the direction of the applied load. This scheme arrests local collapse and causes it to spread to neighboring material at a nearly constant stress level as in the experiments. The stress picks up again when the whole domain is crushed (densification stage). The extent of the stress plateau is governed by a parameter of the pseudo-contact scheme used.

In conclusion, the results show that the idealized Kelvin cell foam assigned several of the geometric characteristics of the foams tested reproduces some features of the compressive responses well quantitatively and others qualitatively. The initial elastic properties of the anisotropic foam were shown in Part I to be reproduced by the model quite well. The nonlinear responses in the rise and transverse directions of anisotropic foams are different and the events associated with it are different. Both are governed by buckling of the microstructure. In the rise direction buckling involves a long wavelength mode leading to a limit load. After the limit load localized deformation takes place which spreads to the whole specimen at a nearly constant load. In the transverse direction buckling is associated with modes local to the cell. The postbuckling response is a monotone. These general features of the two behaviors were reproduced by the models. The numerical values of the instabilities and of the rise direction stress plateau were generally higher than measured values. The imperfection sensitivity of these characteristic stresses indicates that better quantitative prediction may require a more accurate modeling of the irregularities in the cell morphology of actual foams. Urethane foams are viscoelastic. Future extensions of this class of models must also account for this type of rate dependence of the base material.

Acknowledgments

The financial support of the National Science Foundation through Grant CMS-0245485 and the Air Force Office of Scientific Research through Grant No. F49620-98-1-0145 is acknowledged with thanks. The authors wish to thank Foamex International Inc. for providing foam samples and technical information on their products and Nick Triantafyllidis for his assistance in tailoring the Bloch wave theory to this problem.

References

Bastawros, A.-F., Bart-Smith, H., Evans, A.G., 2000. Experimental analysis of deformation mechanisms in a closed-cell aluminum alloy foam. J. Mech. Phys. Solids 48, 301–322.

Geymonat, G., Müller, S., Triantafyllidis, N., 1993. Homogenization of nonlinearly elastic materials, microscopic bifurcation and macroscopic loss of rank-one convexity. Arch. Rat. Mech. Anal. 122, 231–290.

Gong, L., Kyriakides, S., Triantafyllidis, N., submitted for publication. On the stability of Kelvin cell fomas under compressive loads. J. Mech. Phys. Solids.

Laroussi, M., Sab, K., Alaoui, A., 2002. Foam mechanics: nonlinear response of an elastic 3D-periodic microstructure. Int. J. Solids Struct. 39, 3599–3623.

Schraad, M.W., Triantafyllidis, N., 1997a. Scale effects in media with periodic and nearly periodic microstructures. Part I: Macroscopic properties. ASME J. Appl. Mech. 64, 751–762.

Schraad, M.W., Triantafyllidis, N., 1997b. Scale effects in media with periodic and nearly periodic microstructures. Part II: Failure mechanisms. ASME J. Appl. Mech. 64, 763–771.

Wang, Y., Gioia, G., Cuitino, A.M., 2000. The deformation habits of compressed open-cell solid foams. ASME J. Eng. Mater. Technol. 122, 376–378.